 CMES, vol.4, no.5, pp.519-534, 2003

Free and Forced Vibrations of Thick Rectangular Plates using Higher-Order Shear and Normal Deformable Plate Theory and Meshless Petrov-Galerkin (MLPG) Method

L. F. Qian[1,2], R. C. Batra[3] and L. M. Chen[1]

Abstract: We use a meshless local Petrov-Galerkin (MLPG) method to analyze three-dimensional infinitesimal elastodynamic deformations of a homogeneous rectangular plate subjected to different edge conditions. We employ a higher-order plate theory in which both transverse shear and transverse normal deformations are considered. Natural frequencies and the transient response to external loads have been computed for isotropic and orthotropic plates. Computed results are found to agree with those obtained from the analysis of the 3-dimensional problem either analytically or by the finite element method.

1 Introduction

Numerical methods used to find an approximate solution of an initial-boundary-value problem include the finite element method (FEM), the finite-difference method, the boundary element method and meshless methods. Advantages of a meshless method over the FEM include the flexibility of placing nodes in the domain of study and not having to connect them to form closed polygons. Out of several meshless methods available in the literature, e.g. see Belytschko et al. (1994), we use here the Meshless Local Petrov-Galerkin (MLPG) method proposed by Atluri and Zhu (1998) and further developed by Atluri et al. (1999, 2000, 2002a,b), Lin and Atluri (2000), and Long and Atluri (2002). Kim and Atluri (2000) and Ching and Batra (2001) used it to analyze plane strain elastostatic deformations of an edge-cracked plate. Warlock et al. (2002) adopted it to study the effect of frictional forces in a contact problem. Gu and Liu (2001) have used the MLPG method to find natural frequencies and forced plane strain deformations of a cantilever beam. Batra and Ching (2002) have delineated the time evolution of the stress-intensity factor in a double edge-cracked plate.

Atluri and Shen (2002a,b) have compared the performance of six variants of the MLPG method for solving Poisson's equation. Qian et al. (2002) used two of these formulations to study elastostatic deformations of a thick rectangular plate with a compatible higher-order shear and normal deformable plate theory (HOSNDPT) proposed by Batra and Vidoli (2002). Batra et al. (2002) have shown that for the same order of the plate theory the mixed HOSNDPT derived from a Hellinger-Reissner principle in which stresses satisfy natural boundary conditions at the major surfaces of the plate gives results closer to the 3-dimensional solution of the problem than the compatible HOSNDPT in which stresses are derived from the assumed displacement field and Hooke's law. However, the compatible HOSNDPT is easier to use than the mixed HOSNDPT. We use the former and the MLPG1 formulation to analyze natural frequencies and the forced transient response of a thick rectangular plate. We compare computed results with those obtained either from the 3-dimensional analysis of the problem by the FEM or available in the literature. In the MLPG1 method, the test function is set equal to the weight function of the moving least squares (MLS) approximation (see Lancaster and Salkauskas (1981)) of the trial solution.

The paper is organized as follows. Sections 2, 3 and 4 briefly review respectively the HOSNDPT, the weak formulation of the problem and the MLPG1 formulation. Section 5 gives results and compares them with those found either from the analysis of the 3-dimensional problem by the FEM or analytical solutions available in the literature. Conclusions are summarized in Section 6.

[1] Nanjing University of Science and Technology
Nanjing 210094, P. R. China
[2] Presently visiting scholar at Virginia Polytechnic Institute and State University
[3] Department of Engineering Science and Mechanics
Virginia Polytechnic Institute and State University, MC 0219
Blacksburg, VA 24061

2 Brief Review of the Compatible HOSNDPT

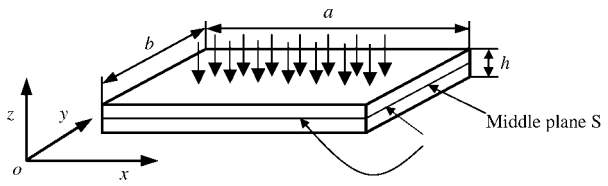

Figure 1 : Schematic sketch of the problem

Figure 1 shows a schematic sketch of the problem studied, the rectangular Cartesian coordinate axes used to describe deformations of the homogeneous plate, and dimensions of the rectangular plate which in the unstressed reference configuration occupies the region $\Omega = [0,a]\times[0,b]\times[-h/2,h/2]$. The midsurface of the plate is denoted by S, the boundary of S by Γ, and displacements of a point along the x, y and z-axes by u, v and w respectively. By using Legendre polynomials in z orthonormalized by

$$\int_{-h/2}^{h/2} L_i(z)L_j(z)dz = \delta_{ij}, \tag{1}$$

we write

$$\mathbf{u}(x,y,z,t) = \left\{\begin{array}{c} u(x,y,z,t) \\ v(x,y,z,t) \\ w(x,y,z,t) \end{array}\right\} = \sum_{i=0}^{K} \left\{\begin{array}{c} u_i(x,y,t) \\ v_i(x,y,t) \\ w_i(x,y,t) \end{array}\right\} L_i(z). \tag{2}$$

In (1), δ_{ij} is the Kronecker delta. Expansion (2) for displacements has been used by Mindlin and Medick (1959) who attributed it to W. Prager, Batra and Vidoli (2002), and Batra et al. (2002). When $K \geq 2$, the plate theory is called higher-order. Equation (2) elucidates that both transverse normal and transverse shear deformations are being considered. Expressions for $L_0(z), L_1(z), \ldots, L_7(z)$ are given in the Appendix. We note that $L_i(z)$ is a polynomial of degree i in z. Hence $L_i'(z) = dL_i/dz$ can be written as

$$L_i'(z) = \sum_{j=0}^{K} d_{ij}L_j(z), \tag{3}$$

where d_{ij} are independent of z. The matrix d_{ij} is given in Batra and Vidoli's (2002) paper for $K = 0,1,2,\ldots,7$ and for $K = 7$ is also listed in the Appendix.

For infinitesimal deformations, strains ε are given by

$$\varepsilon = \left\{\begin{array}{c} \varepsilon_{xx} \\ \varepsilon_{yy} \\ \varepsilon_{zz} \\ 2\varepsilon_{yz} \\ 2\varepsilon_{zx} \\ 2\varepsilon_{xy} \end{array}\right\} = \sum_{i=0}^{K} \left\{\begin{array}{c} \dfrac{\partial u_i(x,y)}{\partial x} \\ \dfrac{\partial v_i(x,y)}{\partial y} \\ \displaystyle\sum_{j=0}^{K} w_j(x,y)d_{ji} \\ \dfrac{\partial w_i(x,y)}{\partial y} + \displaystyle\sum_{j=0}^{K} v_j(x,y)d_{ji} \\ \dfrac{\partial w_i(x,y)}{\partial x} + \displaystyle\sum_{j=0}^{K} u_j(x,y)d_{ji} \\ \dfrac{\partial v_i(x,y)}{\partial x} + \dfrac{\partial u_i(x,y)}{\partial y} \end{array}\right\} L_i(z) \equiv \sum_{i=0}^{K} \{\eta_i\} L_i(z), \tag{4}$$

where for $i = 0,1,2,\ldots,K$, η_i is a 6-dimensional vector with components given by

$$\begin{aligned} &\eta_{i(1)} = \partial u_i/\partial x,\ \eta_{i(2)} = \partial v_i/\partial y,\ \eta_{i(3)} = \sum_{j=0}^{K} d_{ji}w_j, \\ &\eta_{i(4)} = \partial w_i/\partial y + \sum_{j=0}^{K} v_j d_{ji},\ \eta_{i(5)} = \partial w_i/\partial x + \sum_{j=0}^{K} u_j d_{ji}, \\ &\eta_{i(6)} = \partial v_i/\partial x + \partial u_i/\partial y. \end{aligned} \tag{5}$$

Since $d_{ij} \not\equiv 0$, the transverse normal and the transverse shear strains for $K > 1$ depend upon displacements $u_0, v_0, w_0, u_1, v_1, w_1, \ldots u_{K-1}, v_{K-1}, w_{K-1}$. Using Hooke's law, stresses at a point $\mathbf{x} = (x,y,z)$ are given by

$$\sigma = \{\sigma_{xx}\ \ \sigma_{yy}\ \ \sigma_{zz}\ \ \sigma_{yz}\ \ \sigma_{zx}\ \ \sigma_{xy}\}^T = \mathbf{D}\varepsilon, \tag{6}$$

where $\mathbf{D}$ is the matrix of elastic constants. The plate has been assumed to be initially stress free. Substitution from (4) and (5) into (6) gives stresses at the point $\mathbf{x}$ in terms of displacements and in-plane gradients of displacements of the point (x,y) on the midsurface S.

We omit here derivation of the plate equations which are given in Batra and Vidoli (2002) for a piezoelectric plate based on the mixed variational principle of Yang and Batra (1995) and in Batra et al. (2002) for an elastic plate based on the Hellinger-Reissner principle. The weak formulation of the problem used here is described below.

Denoting the velocity of a point by $\dot{\mathbf{u}}$ and the acceleration

by $\ddot{\mathbf{u}}$, it follows from equation (2) that

$$\dot{\mathbf{u}}(x,y,z,t)=\left\{\begin{array}{c}\dot{u}(x,y,z,t)\\ \dot{v}(x,y,z,t)\\ \dot{w}(x,y,z,t)\end{array}\right\}=\sum_{i=0}^{K}\left\{\begin{array}{c}\dot{u}_i(x,y,t)\\ \dot{v}_i(x,y,t)\\ \dot{w}_i(x,y,t)\end{array}\right\}L_i(z), \tag{7}$$

and a similar expression holds for $\ddot{\mathbf{u}}$. Knowing $\dot{\mathbf{u}}(x,y,z,0)$, $\dot{u}_i(x,y,0)$, $\dot{v}_i(x,y,0)$ and $\dot{w}_i(x,y,0)$ can be computed from (7) by multiplying both sides with $L_j(z)$ and integrating the resulting expression with respect to z from $-h/2$ to $h/2$.

3 Weak Formulation of the Problem

In the absence of body forces, equations governing transient deformations of the plate are

$$\begin{aligned}
\operatorname{div}\boldsymbol{\sigma}&=\rho\ddot{\mathbf{u}} \quad \text{in } \Omega\times(0,T),\\
\boldsymbol{\sigma}\mathbf{n}&=\overline{\mathbf{f}} \quad \text{on } \Gamma_f\times\left[-\frac{h}{2},\frac{h}{2}\right]\times(0,T),\\
\mathbf{u}&=\overline{\mathbf{u}} \quad \text{on } \Gamma_u\times\left[-\frac{h}{2},\frac{h}{2}\right]\times(0,T),\\
\boldsymbol{\sigma}\mathbf{n}&=\mathbf{q}^{\pm} \quad \text{on } S^{\pm}\times(0,T),\\
\mathbf{u}(x,y,z,0)&=\mathbf{u}^0(x,y,z) \text{ in } \Omega,\\
\dot{\mathbf{u}}(x,y,z,0)&=\dot{\mathbf{u}}^0(x,y,z) \text{ in } \Omega.
\end{aligned} \tag{8}$$

Equation $(8)_1$ expresses the balance of linear momentum, equations $(8)_2$-$(8)_4$ boundary conditions, and equations $(8)_5$ and $(8)_6$ initial conditions. Here ρ is the mass density, div the three-dimensional divergence operator, $\mathbf{n}$ is an outward unit normal to the surface, and a superimposed dot denotes partial derivative with respect to time t. S^+ and S^- are the top and the bottom surfaces of the plate where surface tractions are prescribed respectively as $\boldsymbol{q}^+$ and $\boldsymbol{q}^-$. Γ_u and Γ_f are parts of the boundary ∂S of S. On the edge surfaces of the plate, displacements and surface tractions are prescribed as $\overline{\mathbf{u}}$ and $\overline{\mathbf{f}}$ on $\Gamma_u\times\left[-\frac{h}{2},\frac{h}{2}\right]$ and $\Gamma_f\times\left[-\frac{h}{2},\frac{h}{2}\right]$ respectively.

Let $\tilde{u}$, $\tilde{v}$ and $\tilde{w}$ be three linearly independent functions defined on Ω. Like u, v and w in eqn. (2), $\tilde{u}$, $\tilde{v}$ and $\tilde{w}$ are expanded in terms of Legendre polynomials in z. Multiplying the three equations $(8)_1$ expressing the balance of linear momentum in x, y, and z directions by $\tilde{u}$, $\tilde{v}$ and $\tilde{w}$ respectively, adding the three resulting equations, and using the divergence theorem, we obtain

$$\int_\Omega \tilde{\boldsymbol{\varepsilon}}^T\boldsymbol{\sigma}d\Omega-\int_{\partial\Omega}\tilde{\mathbf{u}}^T\boldsymbol{\sigma}\mathbf{n}dS+\int_\Omega\rho\tilde{\mathbf{u}}^T\ddot{\mathbf{u}}d\Omega=0. \tag{9}$$

Here $\tilde{\boldsymbol{\varepsilon}}$ is the 6-dimensional strain vector derived from displacements $\tilde{\mathbf{u}}=(\tilde{u},\tilde{v},\tilde{w})$, and $\partial\Omega$ is the boundary of Ω. Substitution from (4), (6), and $(8)_2$-$(8)_4$ into (9) and integration with respect to z from $-h/2$ to $h/2$ give

$$\begin{aligned}
\sum_{i=0}^{K}\Bigg[&\int_S\{\tilde{\eta}_i\}[D]\{\eta_i\}dS-\int_{\Gamma_u}\{\tilde{u}_i\}^T[n][D]\{\eta_i\}d\Gamma\\
&-\int_{\Gamma_f}\{\tilde{u}_i\}^T\{\overline{f}_i\}d\Gamma+\int_S\{\tilde{u}_i\}^T\rho\{\ddot{u}_i\}dS\\
&-L_i\left(\pm\frac{h}{2}\right)\int_S\{\tilde{u}_i\}^T\{q^{\pm}\}dS\Bigg]=0,
\end{aligned} \tag{10}$$

where

$$\{\overline{f}_i\}=\int_{-h/2}^{h/2}L_i(z)\{\overline{f}\}dz. \tag{11}$$

In the Galerkin formulation of the problem $\{\tilde{u}_i\}$ is usually taken to vanish on Γ_u. However, in the MLPG formulation, it is not necessary to do so since essential boundary conditions are imposed either by the penalty method or by the elimination of the corresponding degrees of freedom or by the method of Lagrange multipliers.

4 Implementation of the MLPG Method

4.1 Semidiscrete formulation

Let M nodes be placed on S, and $S_1,S_2,\ldots,S_M$ be smooth two-dimensional closed regions enclosing nodes $1,2,\ldots,M$ respectively such that $\bigcup_{\alpha=1}^{M}S_\alpha=S$. $S_1,S_2,\ldots,S_M$ need not be of the same shape and size, and the intersection of any two or more of them need not be empty. Let $\phi_1,\phi_2,\ldots,\phi_N$ and $\psi_1,\psi_2,\ldots,\psi_N$ be linearly independent functions defined on S_α. For a Kth order plate theory there are $3(K+1)$ unknowns $\mathbf{u}_0,\mathbf{u}_1,\ldots,\mathbf{u}_K$ at a point in S_α. We write these as a $3(K+1)$ dimensional array $\{u\}$, and set

$$\{u(x,y,t)\}=\sum_{J=1}^{N}[\phi_J(x,y)]\{\delta_J(t)\}, \tag{12}$$

$$\{\tilde{u}(x,y)\}=\sum_{J=1}^{N}[\psi_J(x,y)]\{\tilde{\delta}_J\}, \tag{13}$$

where, for each value of J, $\{\delta_J\}$ is a $3(K+1)$ dimensional array and $\{\phi_J\}$ is a square matrix of $3(K+1)$ rows; similar remarks apply to $\{\tilde{u}\}$, $[\psi_J]$ and $\{\tilde{\delta}_J\}$. Note that

δ_J vary with time t. The $3(K+1)\times 3(K+1)$ matrix $\{\phi_J\}$ can be divided into $(K+1)$ submatrices each of size $3\times 3(K+1)$. The ith such submatrix is given by

$$[i\text{th submatrix of } \phi_J] = \left[\begin{array}{ccccccccccc} \overbrace{} & & & & \overbrace{} & & & & \overbrace{} & & \\ 0 & 0 & 0 & \dots & \phi_J & 0 & 0 & \dots & 0 & 0 & 0 \\ 0 & 0 & 0 & \dots & 0 & \phi_J & 0 & \dots & 0 & 0 & 0 \\ 0 & 0 & 0 & \dots & 0 & 0 & \phi_J & \dots & 0 & 0 & 0 \end{array}\right] \begin{array}{c} {\scriptstyle 0} \\ \\ \\ \end{array} \begin{array}{c} {\scriptstyle i} \\ \\ \\ \end{array} \begin{array}{c} {\scriptstyle K} \\ \\ \\ \end{array} \quad (14)$$

Note that the location of the 3×3 diagonal matrix $\phi_J I$, where I is a 3×3 unit matrix, depends upon the value of i. For example, for $i=0$, $\phi_J I$ occupies the first three rows and columns of $[\phi_J]$; for $i=1$, the second three rows and columns etc. The analogue of unknowns $\{\delta_J\}$ is the nodal displacements in the FEM. However, in the MLPG method, $\{\delta_J\}$ do not generally equal nodal displacements. Substitution from (12) and (13) into (5) gives

$$\{\eta\} = \sum_{J=1}^{N} [B_J]\{\delta_J\},\ \{\tilde{\eta}\} = \sum_{J=1}^{N} [\tilde{B}_J]\{\tilde{\delta}_J\}, \quad (15)$$

where $\{\eta\}$ is a $6(K+1)$ dimensional array and B is a $6(K+1)\times 3(K+1)$ matrix which can be divided into $(K+1)$ submatrices each of size $6\times 3(K+1)$. The ith such submatrix is given by

$$[i\text{th submatrix of } B_J] = \left[\begin{array}{ccccccccccc} \overbrace{} & & & & \overbrace{} & & & & \overbrace{} & & \\ 0 & 0 & 0 & .. & \partial\phi_J/\partial x & 0 & 0 & .. & 0 & 0 & 0 \\ 0 & 0 & 0 & .. & 0 & \partial\phi_J/\partial y & 0 & .. & 0 & 0 & 0 \\ 0 & 0 & \phi_J d_{0i} & .. & 0 & 0 & \phi_J d_{ii} & .. & 0 & 0 & \phi_J d_{Ki} \\ 0 & \phi_J d_{0i} & 0 & .. & 0 & \phi_J d_{ii} & \partial\phi_J/\partial y & .. & 0 & \phi_J d_{Ki} & 0 \\ \phi_J d_{0i} & 0 & 0 & .. & \phi_J d_{ii} & 0 & \partial\phi_J/\partial x & .. & \phi_J d_{Ki} & 0 & 0 \\ 0 & 0 & 0 & .. & \partial\phi_J/\partial y & \partial\phi_J/\partial x & 0 & .. & 0 & 0 & 0 \end{array}\right] \begin{array}{c} {\scriptstyle 0} \\ \\ \\ \\ \\ \\ \end{array} \begin{array}{c} {\scriptstyle i} \\ \\ \\ \\ \\ \\ \end{array} \begin{array}{c} {\scriptstyle K} \\ \\ \\ \\ \\ \\ \end{array} \quad (16)$$

where the repeated index i in d_{ii} is not summed. The matrix $\tilde{B}_J$ is obtained from B_J by substituting ψ_J for ϕ_J.

We now replace the domain of integration S in equation (10) by S_α, substitute for $\{\eta\}$, $\{\tilde{\eta}\}$, $\{u\}$ and $\{\tilde{u}\}$ from equations (12), (13) and (15), require that the resulting equation hold for all choices of $\{\tilde{\delta}\}$, and arrive at the following system of coupled ordinary differential equations (ODEs).

$$[K_{IJ}]\{\delta_J\} + [M_{IJ}]\{\ddot{\delta}_J\} = \{F_I\}. \quad (17)$$

Here

$$[K_{IJ}] = \int_{S_\alpha} \left([\tilde{B}_I]^T [D][B_J]\right) dS - \int_{\Gamma_{\alpha u}} \left([\psi_I]^T [n][D][B_J]\right) d\Gamma - \int_{\Gamma_{\alpha 0}} \left([\psi_I]^T [n][D][B_J]\right) d\Gamma, \quad (18)$$

$$\{F_I\} = \int_{S_\alpha} [\psi_I]^T \{\overline{q}\} dS + \int_{\Gamma_{\alpha f}} [\psi_I]^T \{\overline{f}_i\} d\Gamma + L_i(\pm h/2) \int_{S_\alpha} [\psi_I]^T \{q^{\pm}\} dS, \quad (19)$$

$$[M_{IJ}] = \int_{S_\alpha} \rho [\psi_I]^T [\phi_J] dS, \quad (20)$$

where $\Gamma_{\alpha 0} = \partial S_\alpha - \Gamma_{\alpha u} - \Gamma_{\alpha f}$, $\Gamma_{\alpha u} = \partial S_\alpha \cap \Gamma_u$, $\Gamma_{\alpha f} = \partial S_\alpha \cap \Gamma_f$. The matrix $[K_{IJ}]$ is usually called the stiffness matrix, $[M_{IJ}]$ the mass matrix, and $\{F_I\}$ the load vector. For the MLPG formulation, M and K need not be symmetric and K may not be positive definite even after essential boundary conditions have been imposed. Equations like (17) are derived for each S_α, $\alpha = 1,2,\dots,M$. Initial conditions on $\{\delta_J\}$ are obtained by substituting from (12), $(8)_5$ and $(8)_6$ into (7) and following the procedure outlined after equation (7). For $\mathbf{u}^0 = \mathbf{0} = \dot{\mathbf{u}}^0$, $\{\delta_J(0)\}$ and $\{\dot{\delta}_J(0)\}$ are null matrices. Essential boundary conditions $(8)_3$ are satisfied by following the procedure outlined in section 4.3.

For a free vibration problem, $\{F_I\} = \{0\}$ and

$$\{\delta_J(t)\} = e^{i\omega t}\{\overline{\delta}_J\}, \quad (21)$$

where $\{\overline{\delta}_J\}$ is the amplitude vector and ω a natural frequency. Thus natural frequencies are given by

$$\det\left[[K_{IJ}] - \omega^2 [M_{IJ}]\right] = 0 \quad (22)$$

and the corresponding mode shapes $\{\overline{\delta}_J\}$ can be computed from

$$[K_{IJ}]\{\overline{\delta}_J\} = \omega^2 [M_{IJ}]\{\overline{\delta}_J\} \quad (23)$$

by imposing a suitable normalization constraint on $\{\overline{\delta}_J\}$.

In order to complete the formulation of the problem, we now describe briefly the moving least squares (MLS) approximation (see Lancaster and Salkauskas (1981)) for details) for finding basis functions $\{\phi_J\}$, and the technique to impose essential boundary conditions.

4.2 Brief Description of the MLS Basis Functions

In the MLS method, the approximation $f^h(x,y,t)$ of a scalar-valued function $f(x,y,t)$ defined on S_α is written

as

$$f^h(x,y,t) = \sum_{j=1}^{m} p_j(x,y)a_j(x,y,t), \tag{24}$$

where

$$\mathbf{p}^T(x,y) = \{1,x,y,x^2,xy,y^2,\ldots\}, \tag{25}$$

is a complete monomial in (x,y) having m terms. For complete monomials of degrees 1, 2 and 3, $m = 3$, 6 and 10 respectively. The unknown coefficients $a_1, a_2, \ldots, a_m$ are functions of $\mathbf{x} = (x,y)$ and time t, and are determined by minimizing J defined by

$$J = \sum_{i=1}^{n} W(\mathbf{x}-\mathbf{x}_i)[\mathbf{p}^T(\mathbf{x}_i)\mathbf{a}(\mathbf{x},t) - \hat{f}_i(t)]^2, \tag{26}$$

where $\hat{f}_i(t)$ is the fictitious value at time t of f at the point (x_i,y_i), and n is the number of points in the domain of influence of $\mathbf{x}$ for which the weight function $W(\mathbf{x}-\mathbf{x}_i) > 0$. We take

$$W(\mathbf{x}-\mathbf{x}_i) = \begin{cases} 1-6\left(\dfrac{d_i}{r_w}\right)^2+8\left(\dfrac{d_i}{r_w}\right)^3-3\left(\dfrac{d_i}{r_w}\right)^4, & 0 \le d_i \le r_w, \\ 0, & d_i \ge r_w, \end{cases} \tag{27}$$

where $d_i = |\mathbf{x}-\mathbf{x}_i|$ is the distance between points $\mathbf{x}$ and $\mathbf{x}_i$, and r_w is the size of the support of the weight function W. Thus the support of W is a circle of radius r_w with center at the point $\mathbf{x}_i$.

The stationarity of J with respect to $\mathbf{a}(\mathbf{x},t)$ gives the following system of linear equations for the determination of $\mathbf{a}(\mathbf{x},t)$:

$$\mathbf{A}(\mathbf{x})\mathbf{a}(\mathbf{x},t) = \mathbf{B}(\mathbf{x})\hat{\mathbf{f}}(t), \tag{28}$$

where

$$\begin{aligned} \mathbf{A}(\mathbf{x}) &= \sum_{i=1}^{n} W(\mathbf{x}-\mathbf{x}_i)\mathbf{p}^T(\mathbf{x}_i)\mathbf{p}(\mathbf{x}_i), \\ \mathbf{B}(\mathbf{x}) &= [W(\mathbf{x}-\mathbf{x}_1)\mathbf{p}(\mathbf{x}_1),\ W(\mathbf{x}-\mathbf{x}_2)\mathbf{p}(\mathbf{x}_2),\ldots, \\ &\qquad W(\mathbf{x}-\mathbf{x}_n)\mathbf{p}(\mathbf{x}_n)]. \end{aligned} \tag{29}$$

Substitution for $\mathbf{a}(\mathbf{x},t)$ from (28) into (24) gives

$$f^h(\mathbf{x},t) = \sum_{j=1}^{m} \phi_j(\mathbf{x})\,\hat{f}_j(t), \tag{30}$$

where

$$\phi_k(\mathbf{x}) = \sum_{j=1}^{m} p_j(\mathbf{x})[\mathbf{A}^{-1}(\mathbf{x})\mathbf{B}(\mathbf{x})]_{jk}, \tag{31}$$

may be considered as the basis functions of the MLS approximation. It is clear that $\phi_k(x_j)$ need not equal the Kronecker delta δ_{kj}. In order for the matrix $\mathbf{A}$, defined by $(29)_1$, to be invertible, the number n of points in the domain of influence of $\mathbf{x}$ must at least equal m. For m equal to 3 or 6, Chati and Mukherjee (2000) have found that $15 \le n \le 30$ gives acceptable results for two-dimensional elastostatic problems. For a two-dimensional elastodynamic problem, Batra and Ching (2002) used Gauss weight functions, the complete set of quadratic monomials and $r_w = 3.5$ times the distance to the third node nearest to the node at $\mathbf{x}_i$. Thus r_w and the locations of nodes in S_α and hence S must be such that n satisfies the required constraint. We take

$$r_w = ch_i \tag{32}$$

where h_i is the distance from node i to its nearest neighbor and c is a scaling parameter.

In Atluri and Shen's (2002a,b) terminology we use the MLPG1 formulation and set $\psi_J = W(\mathbf{x}-\mathbf{x}_J)$ with $r_w = h_J$. Thus the support of ψ_J is a circle centered at $\mathbf{x}_J$ and radius equal to the distance from $\mathbf{x}_J$ to the nearest node.

4.3 Matrix Transformation Technique for Satisfying Essential Boundary Conditions

We use the matrix transform technique to satisfy essential boundary conditions. In this subsection, the dependence on time is not explicitly indicated. Let D and I denote respectively the set of nodes where x-displacements are and are not prescribed; a similar procedure is used for y- and z-displacements. Writing the x-displacements of all nodes as $\{u\}$, we have

$$\{u\} = \begin{Bmatrix} u_D \\ u_I \end{Bmatrix} = \begin{bmatrix} \phi_{DD} & \phi_{DI} \\ \phi_{ID} & \phi_{II} \end{bmatrix} \begin{Bmatrix} \delta_D \\ \delta_I \end{Bmatrix}. \tag{33}$$

Solving the first of these equations for δ_D, we obtain

$$\{\delta\} = \begin{Bmatrix} \delta_D \\ \delta_I \end{Bmatrix} = \begin{Bmatrix} \phi_{DD}^{-1}u_D \\ 0 \end{Bmatrix} + \begin{bmatrix} -\phi_{DD}^{-1}\phi_{DI} \\ I \end{bmatrix} \{\delta_I\}, \tag{34}$$

where 0 and I are the null and the identity matrices respectively. Substitution from (34) into (17)

and the premultiplication of the resulting equation by $\begin{bmatrix} -\psi_{DD}^{-1}\psi_{DI} \\ I \end{bmatrix}^T$ give

$$[\overline{K}_{IJ}]\{\delta_J\}+[\overline{M}_{IJ}]\{\ddot{\delta}_J\}=\{\overline{F}_I\}, \tag{35}$$

where

$$\begin{aligned}
[\overline{K}_{IJ}] &= \begin{bmatrix} -\psi_{DD}^{-1}\psi_{DI} \\ I \end{bmatrix}^T [K_{IJ}] \begin{bmatrix} -\phi_{DD}^{-1}\phi_{DI} \\ I \end{bmatrix}, \\
[\overline{M}_{IJ}] &= \begin{bmatrix} -\psi_{DD}^{-1}\psi_{DI} \\ I \end{bmatrix}^T [M_{IJ}] \begin{bmatrix} -\phi_{DD}^{-1}\phi_{DI} \\ I \end{bmatrix}, \\
\{\overline{F}_I\} &= \begin{bmatrix} -\psi_{DD}^{-1}\psi_{DI} \\ I \end{bmatrix}^T \{F_I\} - \begin{bmatrix} -\psi_{DD}^{-1}\psi_{DI} \\ I \end{bmatrix}^T [K_{IJ}] \begin{Bmatrix} \phi_{DD}^{-1}u_D \\ 0 \end{Bmatrix} \\
&\quad - \begin{bmatrix} -\psi_{DD}^{-1}\psi_{DI} \\ I \end{bmatrix}^T [M_{IJ}] \begin{Bmatrix} \phi_{DD}^{-1}\ddot{u}_D \\ 0 \end{Bmatrix}.
\end{aligned} \tag{36}$$

For the free vibration problem matrices $[K_{IJ}]$ and $[M_{IJ}]$ in equations (22) and (23) can be similarly modified.

4.4 Numerical Integration of ODEs

Two techniques, namely, the Newmark family of methods and the Wilson-θ method have been employed to integrate equations (35) subject to the initial conditions. In the Newmark family of methods, displacements $\delta^{t+\Delta t}$ and velocities $\dot{\delta}^{t+\Delta t}$ at time $t+\Delta t$ are related to their values at time t by

$$\begin{aligned}
\delta^{t+\Delta t} &= \delta^t + \Delta t\dot{\delta}^t + \frac{(\Delta t)^2}{2}((1-2\beta)\ddot{\delta}^t + 2\beta\ddot{\delta}^{t+\Delta t}), \\
\dot{\delta}^{t+\Delta t} &= \dot{\delta}^t + \Delta t((1-\gamma)\ddot{\delta}^t + \gamma\ddot{\delta}^{t+\Delta t}),
\end{aligned} \tag{37}$$

where parameters β and γ control the accuracy and the stability of the integration scheme and Δt is the uniform time increment. The Newmark family of methods is unconditionally stable if

$$\gamma \geq \frac{1}{2} \text{ and } \beta \geq \frac{1}{4}\left(\frac{1}{2}+\gamma\right)^2 \tag{38}$$

and second-order accurate for $\gamma = \frac{1}{2}$ only; otherwise it is first-order accurate. Here we use $\gamma = 0.5$ and $\beta = 0.25$; thus the integration scheme is unconditionally stable and non-dissipative. A way to use this algorithm is to solve equations (35) for $\ddot{\delta}^{t+\Delta t}$ and then find $\delta^{t+\Delta t}$ and $\dot{\delta}^{t+\Delta t}$ from (37) and the known solution at time t. One can thus march forward in time.

The Wilson-θ method assumes that the acceleration varies linearly in the time interval $[t, \quad t+\theta\Delta t]$ where $\theta \geq 1$ and is usually taken as 1.37. Thus

$$\begin{aligned}
\ddot{\delta}^{t+\theta\Delta t} &= (1-\theta)\ddot{\delta}^t + \theta\ddot{\delta}^{t+\Delta t}, \\
\dot{\delta}^{t+\theta\Delta t} &= \dot{\delta}^t + \frac{\theta^2\Delta t}{2}\ddot{\delta}^{t+\Delta t} + \left(\frac{2}{\theta}-1\right)\frac{\theta^2\Delta t}{2}\ddot{\delta}^t, \\
\delta^{t+\theta\Delta t} &= \delta^t + \theta\Delta t\dot{\delta}^t + \frac{3-\theta}{6}\theta^2\Delta t^2\ddot{\delta}^t + \frac{\theta^3\Delta t^2}{6}\ddot{\delta}^{t+\Delta t}.
\end{aligned} \tag{39}$$

The method is unconditionally stable for $\theta \geq 1.37$. Equations (35) are written at time $t+\theta\Delta t$, equations $(39)_1$ are used and the resulting equations are solved for $\ddot{\delta}^{t+\Delta t}$. Then equations (40) are used to evaluate $\delta^{t+\Delta t}$ and $\dot{\delta}^{t+\Delta t}$.

$$\begin{aligned}
\delta^{t+\Delta t} &= \delta^t + \dot{\delta}^t\Delta t + (2\ddot{\delta}^t + \ddot{\delta}^{t+\Delta t})\frac{\Delta t^2}{6} \\
\dot{\delta}^{t+\Delta t} &= \dot{\delta}^t + (\ddot{\delta}^{t+\Delta t} + \ddot{\delta}^t)\frac{\Delta t}{2}.
\end{aligned} \tag{40}$$

5 Computation and Discussion of Results

When computing numerical results the region S_α associated with node α is set equal to a circle of radius h_α with center at $\mathbf{x}_\alpha$; it preserves the local character of the MLPG formulation. Integrals appearing in equations (18)-(20) are evaluated by using a 9×9 Gauss quadrature rule. The MLS basis functions ϕ_J in equation (31) are found for each Gauss quadrature point $\mathbf{x}_Q$.

The following boundary conditions are imposed at a simply supported (S), a clamped (C) and a free (F) edge.

$$\begin{aligned}
S:&\ \sigma_{xx}=0,\ v=w=0 \text{ on } x=0,a; \\
&\ \sigma_{yy}=0,\ u=w=0 \text{ on } y=0,b; \\
C:&\ u=v=w=0 \text{ on } x=0,a;\ y=0,b; \\
F:&\ \sigma_{xx}=\sigma_{yx}=\sigma_{zx}=0 \text{ on } x=0,a; \\
&\ \sigma_{yy}=\sigma_{xy}=\sigma_{zy}=0 \text{ on } y=0,b.
\end{aligned} \tag{41}$$

Henceforth S will be used to denote a simply supported edge and not the midsurface.

Unless otherwise noted, we have set $c=15$, $K=5$, $M=196$ and $m=15$. Complete monomials of degree 4 are employed to generate the MLS basis functions. Equal number of nodes, as shown in Fig. 2, are uniformly placed in the x and y-directions.

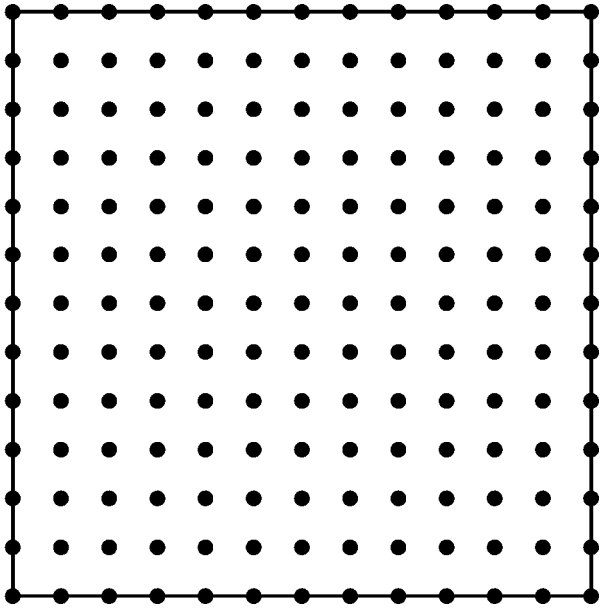

Figure 2 : Locations of uniformly distributed nodes on the midsurface

5.1 Natural Frequencies

We compute natural frequencies of a homogeneous plate made of either an isotropic or an orthotropic material and compare them with either the analytical solution of Srinivas and Rao (1970) as augmented by Batra and Aimmanee (2003) or with those obtained by the analysis of the 3-dimensional problem with the FEM and/or with results available in the literature. Srinivas and Rao (1970) found analytically frequencies of vibrations of a simply supported plate by assuming that

$$\begin{aligned} u(x,y,z,t) &= \sum_{m,n=1}^{\infty} e^{i\omega_{mn}t} U_{mn}(z) \cos\frac{m\pi x}{a}\sin\frac{n\pi y}{b}, \\ v(x,y,z,t) &= \sum_{m,n=1}^{\infty} e^{i\omega_{mn}t} V_{mn}(z) \sin\frac{m\pi x}{a}\cos\frac{n\pi y}{b}, \\ w(x,y,z,t) &= \sum_{m,n=1}^{\infty} e^{i\omega_{mn}t} W_{mn}(z) \sin\frac{m\pi x}{a}\sin\frac{n\pi y}{b}. \end{aligned} \tag{42}$$

For an isotropic simply supported plate, Batra and Aimmanee (2003) have recently found that frequencies

$$\omega_{mn} = \left(\frac{m^2\pi^2}{a^2} + \frac{n^2\pi^2}{b^2}\right)^{1/2}\sqrt{\frac{G}{\rho}}, \tag{43}$$

of the in-plane vibration mode shapes

$$\begin{aligned} u(x,y,z) &= U_{mn}\cos\frac{m\pi x}{a}\sin\frac{n\pi y}{b}, \\ v(x,y,z) &= V_{mn}\sin\frac{m\pi x}{a}\cos\frac{n\pi y}{b}, \\ w(x,y,z) &= 0. \end{aligned} \tag{44}$$

when either $m = 0$ or $n = 0$ were missed by Srinivas and Rao. In equation (43) G is the shear modulus. The amplitudes U_{mn} and V_{mn} of in-plane modes satisfy the constraint

$$bU_{mn}m + aV_{mn}n = 0. \tag{45}$$

For either $m = 0$ or $n = 0$, the amplitudes U_{on} and V_{m0} are unconstrained.

The frequency equation (22) is solved by the three-term look-ahead Lanczos algorithm developed by Freund (1994). This method was found to be more accurate and efficient than some of the others we tried.

Results are presented in terms of the nondimensional frequency $\overline{\omega}$ related to the dimensional frequency ω by

$$\overline{\omega} = \omega h\sqrt{\frac{\rho}{E}}, \tag{46}$$

where E is Young's modulus. For an isotropic square plate with $a = 250$ *mm*, $h/a = 0.1$, and Poisson's ratio = 0.3, Table 1 compares the presently computed flexural frequencies with those obtained by other researchers and also by the FE analysis of the three-dimensional problem with the commercial code IDEAS. The FE results were computed with a uniform $40\times40\times4$ 20-node brick element mesh with 4 elements in the thickness direction. We employed the consistent mass matrix with both the FE and the MLPG formulations. It is clear that the MLPG results agree very well with those of other researchers. Kant's (2001) results are based on his model 2. A shear correction factor of $5/6$ is used in computing results with the Whitney-Pagano's theory. However, no such correction factor is used in the present compatible HOSNDPT.

Frequencies listed in Table 1 are not the 13 lowest frequencies but are frequencies corresponding to the flexural modes of vibration signified by the values of m and n. These are identified by looking at the mode shapes computed with the FEM. The first 10 lowest frequencies of a simply supported square plate with $h/a = 0.1, 0.2, 0.3, 0.4$ and 0.5 obtained with the MLPG and the

Table 1 : Natural frequencies $\overline{\omega} = \omega h\sqrt{\rho/E}$ of a *SSSS* isotropic square plate with $\nu = 0.3$, and $h/a = 0.1$.

No.	m	n	MLPG (Consistent mass)	Srinivas et al. (1970)	Kant et al. (2001)	FEM (I-Deas)	Whitney-Pagano (1970)	Senthilnathan et al. (1987)
1	1	1	0.0578	0.0578	0.0578	0.0577	0.0577	0.0577
2	1	2	0.1391	0.1381	0.1381	0.1379	0.1377	0.1377
3	2	2	0.2133	0.2122	0.2122	0.2118	0.2112	0.2112
4	1	3	0.2606	0.2587	0.2587	0.2583	0.2573	0.2574
5	2	3	0.3214	0.3249	0.3250	0.3242	0.3229	0.3230
6	1	4	0.3973	0.4075	0.4076	0.4063	0.4044	0.4046
7	3	3	0.4226	0.4272	0.4274	0.4259	0.4238	0.4241
8	2	4	0.4651	0.4658	0.4661	0.4643	0.4618	0.4622
9	3	4	0.5456	-	0.5577	0.5548	0.5517	0.5525
10	1	5	0.5632	0.5748	0.5752	0.5723	0.5689	0.5697
11	2	5	0.6154	-	0.6265	0.6148	0.6192	0.6202
12	4	4	0.6909	0.6753	0.6759	-	0.6676	0.6688
13	3	5	0.7066	-	0.7002	-	0.6989	-

Table 2 : First ten natural frequencies $\overline{\omega} = \omega h\sqrt{\rho/E}$ for a *SSSS* isotropic square plate with $\nu = 0.3$. An * indicates the frequency of an in-plane mode of vibration.

No	$h/a = 0.1$			$h/a = 0.2$		$h/a = 0.3$		$h/a = 0.4$		$h/a = 0.5$		
	MLPG	FEM	Batra-Aimmanee (2003)	MLPG	FEM	MLPG	FEM	MLPG	FEM	MLPG	FEM	Batra-Aimmanee (2003)
1	0.0578	0.0578	0.0578	0.2122	0.2122	0.4273	0.4273	0.6753	0.6754	0.9401	0.9403	0.9401
2	0.1391	0.1381	0.1381	0.3897*	0.3897*	0.5845*	0.5845*	0.7793*	0.7793*	0.9741*	0.9742*	0.9742
3	0.1391	0.1381	0.1381	0.3897*	0.3897*	0.5845*	0.5845*	0.7793*	0.7793*	0.9741*	0.9742*	0.9742
4	0.1948*	0.1948*	0.1949	0.4675	0.4659	0.8276*	0.8266*	1.1035*	1.1021*	1.3793*	1.3777*	1.3777
5	0.1948*	0.1948*	0.1949	0.4675	0.4659	0.8733	0.8713	1.3051	1.3028	1.7438	1.7416	1.7406
6	0.2133	0.2122	0.2122	0.5517*	0.5511*	0.8734	0.8713	1.3051	1.3028	1.7438	1.7416	1.7406
7	0.2606	0.2587	0.2587	0.6772	0.6754	1.1698*	1.1690*	1.5598*	1.5587*	1.9497*	1.9483*	1.9483
8	0.2606	0.2587	0.2587	0.7799*	0.7793*	1.1700*	1.1690*	1.5600*	1.5587*	1.9500*	1.9483*	1.9483
9	0.2759*	0.2755*	0.2757	0.7799*	0.7793*	1.2157	1.2133	1.7470*	1.7426*	2.1783*	2.1783*	2.1783
10	0.3214	0.3249	0.3249	0.8014	0.7990	1.3103*	1.3070*	1.7470*	1.7426*	2.1783*	2.1783*	2.1783

Table 3 : Natural frequencies $\overline{\omega} = \omega h\sqrt{\rho/D_{11}}$ of a *SSSS* square orthotropic plate with $h/a = 0.1$ and $D_{11} = 160GPa$

No.	m	n	MLPG (Consistent mass)	Srinivas et al. (1970)	Kant et al. (2001)	FEM (I-Deas)	Whitney-Pagano (1970)	Senthilnathan et al. (1987)
1	1	1	0.0477	0.0474	0.0474	0.0477	0.0476	0.0478
2	1	2	0.1028	0.1033	0.1033	0.1021	0.1041	0.1049
3	2	1	0.1236	0.1188	0.1188	0.1227	0.1188	0.1198
4	2	2	0.1729	0.1694	0.1694	0.1721	0.1698	0.1726
5	1	3	0.1850	0.1888	0.1888	0.1828	0.1905	0.1919
6	3	1	0.2172	0.2180	0.2181	0.2169	0.2178	0.2197
7	2	3	0.2439	0.2475	0.2476	0.2459	0.2485	0.2533
8	3	2	0.2727	0.2624	0.2625	0.2754	0.2623	0.2677
9	1	4	0.3066	0.2969	0.2969	0.2811	0.2994	0.3012
10	4	1	0.3307	0.3319	0.3319	0.3372	0.3340	0.3340
11	3	3	0.3371	0.3320	0.3320	0.3406	0.3321	0.3414
12	2	4	0.3441	0.3476	0.3476	0.3449	0.3491	0.3558
13	4	2	0.3733	0.3707	0.3707	0.3649	0.3698	0.3775

Table 4 : First ten natural frequencies $\overline{\omega} = \omega h\sqrt{\rho/E}$ for a *CCCC* isotropic plate with $\nu = 0.3$.

No	$h/a = 0.1$		$h/a = 0.2$		$h/a = 0.3$		$h/a = 0.4$		$h/a = 0.5$	
	MLPG	FEM	MLPG	FEM	MLPG	FEM	MLPG	FEM	MLPG	FEM
1	0.0999	0.0992	0.3272	0.3260	0.5975	0.5965	0.8780	0.8775	1.1592	1.1595
2	0.1909	0.1896	0.5736	0.5708	0.9908	0.9882	1.4099	1.4080	1.8262	1.8252
3	0.1909	0.1896	0.5736	0.5708	0.9909	0.9882	1.4099	1.4080	1.8262	1.8252
4	0.2673	0.2660	0.7506	0.7496	1.1270	1.1261	1.5036	1.5027	1.8798	1.8790
5	0.3144	0.3137	0.7507	0.7496	1.1271	1.1261	1.5036	1.5027	1.8798	1.8790
6	0.3171	0.3167	0.7706	0.7676	1.3088	1.3054	1.7799	1.7777	2.2251	2.2225
7	0.3749	0.3740	0.8804	0.8760	1.3347	1.3330	1.8499	1.8470	2.3912	2.3891
8	0.3749	0.3740	0.8897	0.8881	1.4766	1.4699	2.0794	2.0713	2.6861	2.6772
9	0.3807	0.3797	0.8897	0.8881	1.5023	1.4915	2.1141	2.1007	2.7111	2.7114
10	0.3807	0.3797	1.0388	1.0403	1.6371	1.6365	2.1777	2.1775	2.7280	2.7127

Table 5 : First ten natural frequencies $\overline{\omega} = \omega h\sqrt{\rho/E}$ for a *SCSC* isotropic plate with $\nu = 0.3$. An * indicates the frequency of an in-plane mode of vibration.

No	$h/a = 0.1$		$h/a = 0.2$		$h/a = 0.3$		$h/a = 0.4$		$h/a = 0.5$	
	MLPG	FEM	MLPG	FEM	MLPG	FEM	MLPG	FEM	MLPG	FEM
1	0.0816	0.0812	0.2747	0.2740	0.5134	0.5129	0.7697	0.7696	0.9741 *	0.9742*
2	0.1507	0.1494	0.3897*	0.3897*	0.5845*	0.5845*	0.7793*	0.7793*	1.0341	1.0344
3	0.1820	0.1808	0.4899	0.4879	0.8978	0.8954	1.3281	1.3256	1.7264	1.7256
4	0.1948*	0.1948*	0.5519	0.5495	0.9614	0.9590	1.3793	1.3775	1.7649	1.7627
5	0.2417	0.2405	0.6895	0.6888	1.0349	1.0341	1.3805	1.3798	1.7997	1.7987
6	0.2674	0.2644	0.7230	0.7205	1.0978	1.0968	1.4586	1.4574	1.8132	1.8117
7	0.3110	0.3103	0.7333	0.7325	1.1699*	1.1690*	1.5599*	1.5587*	1.9498*	1.9483*
8	0.3400	0.3421	0.7799*	0.7793*	1.2586	1.2556	1.8065	1.8038	2.1783	2.1787
9	0.3445	0.3440	0.8117	0.8074	1.3876	1.3888	1.8503	1.8520	2.3130	2.3153
10	0.3635	0.3640	0.8782	0.8722	1.4234	1.4170	2.0457	2.0375	2.3564	2.3541

Table 6 : First ten natural frequencies $\overline{\omega} = \omega h\sqrt{\rho/E}$ for a *CFCF* isotropic plate with $\nu = 0.3$.

No	$h/a = 0.1$		$h/a = 0.2$		$h/a = 0.3$		$h/a = 0.4$		$h/a = 0.5$	
	MLPG	FEM	MLPG	FEM	MLPG	FEM	MLPG	FEM	MLPG	FEM
1	0.0633	0.0629	0.2158	0.2152	0.4047	0.4038	0.6029	0.6024	0.8025	0.8024
2	0.0740	0.0731	0.2448	0.2435	0.4490	0.4478	0.6596	0.6587	0.8681	0.8675
3	0.1186	0.1172	0.3568	0.3557	0.5355	0.5338	0.7143	0.7121	0.8933	0.8905
4	0.1620	0.1609	0.3835	0.3814	0.7038	0.7017	1.0466	1.0455	1.4001	1.3980
5	0.1752	0.1741	0.4939	0.4911	0.8547	0.8520	1.2142	1.2122	1.5692	1.5679
6	0.1783	0.1777	0.5312	0.5272	0.9207	0.9160	1.2809	1.2786	1.6025	1.6000
7	0.2046	0.2081	0.6386	0.6370	0.9595	0.9575	1.3123	1.3100	1.6403	1.6375
8	0.2192	0.2198	0.6469	0.6492	0.9843	0.9826	1.3149	1.3101	1.7099	1.7056
9	0.2912	0.2907	0.6555	0.6531	1.0533	1.0514	1.3992	1.3968	1.7389	1.7359
10	0.3021	0.3008	0.6562	0.6550	1.1384	1.1318	1.5805	1.5785	1.9515	1.9481

FE methods are listed in Table 2 where frequencies of in-plane modes of vibration are marked with an asterisk. Liew et al. (1995) analyzed free vibrations of a thick rectangular plate and listed a few of the in-plane modes of vibration for simply supported edges. It is clear that as the plate gets thicker, more of the in-plane modes of vibration have frequencies lower than the third flexural mode of vibration. For a square plate, $m = 0,\ n = 1$ and $m = 1,\ n = 0$ give the same frequency but have different mode shapes. The in-plane modes of vibration are not predicted by a plate theory, such as the classical one, that neglects u_0 and v_0.

In order to compute natural frequencies of a simply supported orthotropic square plate, we take elastic constants for Aragonite given by Srinivas et al. (1970).

$$\mathbf{D} = \begin{bmatrix} 160 & 37.3 & 1.72 & 0 & 0 & 0 \\ & 86.87 & 15.72 & 0 & 0 & 0 \\ & & 84.81 & 0 & 0 & 0 \\ & & & 25.58 & 0 & 0 \\ & \text{Sym} & & & 42.68 & 0 \\ & & & & & 42.06 \end{bmatrix} \text{ GPa.} \tag{47}$$

Table 3 lists frequencies of different flexural modes obtained by various methods. It is interesting to note that frequencies computed with the MLPG method and employing only 196 nodes are closer to the analytical solution than those obtained with the FEM and much larger number of nodes. For the HOSNDPT, there are $3(K+1)$ unknowns at each node. The number of degrees of freedom in the 3-dimensional FE analysis of the problem is significantly more than that in the MLPG. Batra and Aimmanee (2003) have pointed out that the in-plane modes of vibration (44) are admissible in a simply supported orthotropic plate. However, we did not attempt to find the first 10 natural frequencies.

We have listed in Tables 4-6 the first 10 natural frequencies for an isotropic plate with different edge conditions and $h/a = 0.1, 0.2, 0.3, 0.4$ and 0.5. For each one of these 15 cases, the MLPG solution of the HOSNDPT is very close to the 3-dimensional analysis of the problem by the FEM. Frequencies of in-plane modes of vibration of a SCSC isotropic plate are marked with an asterisk in Table 5; these modes are absent for the other two edge conditions studied.

We now delineate the effect of different parameters on the frequencies computed with the MLPG method for a simply supported isotropic square plate with $h/a = 0.2$.

5.1.1 Order of the Plate Theory

Figure 3 exhibits the dependence of the four flexural or bending frequencies upon the order K of the plate theory. Results were computed by using $9 \times 9 = 81$ Gauss quadrature points and 169 uniformly distributed nodes. These results show that $K = 2$ gives very good results for the first bending frequency, $K = 3$ for the second, $K = 4$ for the third and the fourth. Additional results presented in Tables 1 through 6 revealed that $K = 5$ will give very good results even for plates of aspect ratio $h/a = 0.5$. As noted earlier, the number of unknowns at each point equals $3(K+1)$.

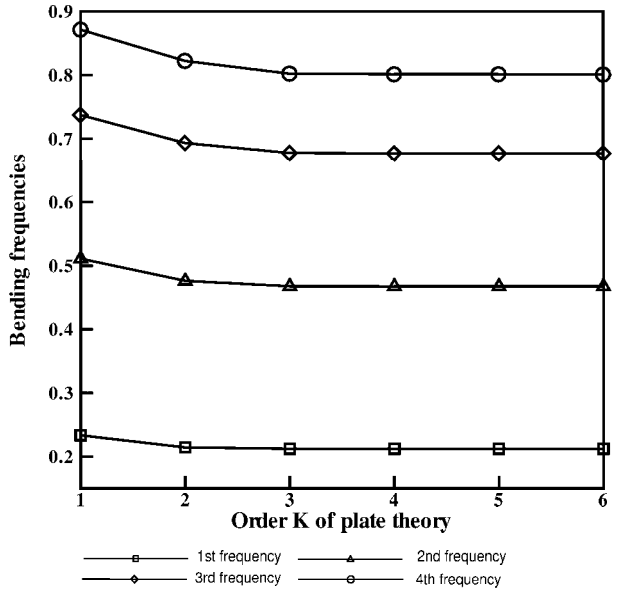

Figure 3 : Bending frequencies of the plate vs. the order K of the plate theory.

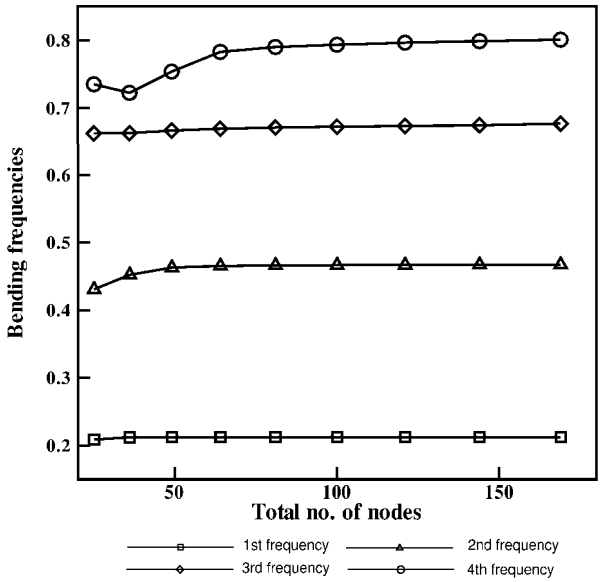

Figure 4 : Convergence of the bending frequency of the plate with the increase in the total number of nodes.

5.1.2 Number of Nodes

For a 5th order plate theory, the dependence of the first four flexural frequencies upon the total number of nodes equispaced in the x- and the y-directions is depicted in Fig. 4. Whereas the first four bending frequencies can be accurately computed with 144 nodes, 169 nodes were needed for obtaining higher frequencies for a square plate of aspect ratio 0.5.

5.1.3 Number of Monomials used to find the MLS basis functions

Since the bending modes for higher frequencies involve more complex deformation fields than those for lower modes, it would seem that more number of monomial terms used to find the MLS basis functions will help. Results plotted in Fig. 5 and additional ones included in Tables 1-6 suggest that $m = 15$ suffices. This value of m corresponds to complete monomials of degree 4.

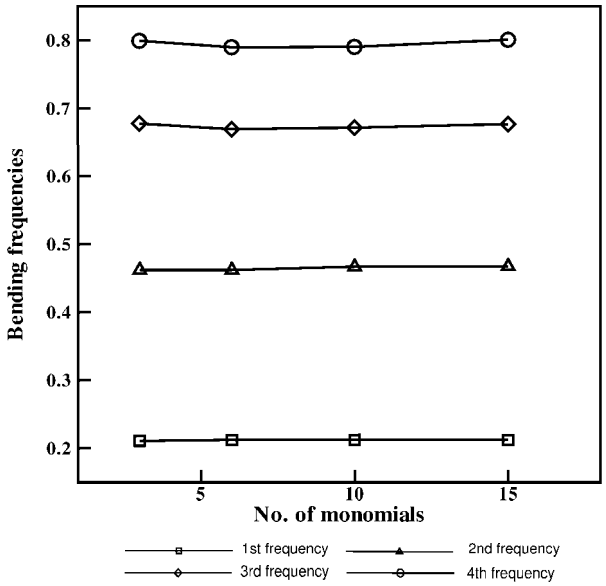

Figure 5 : Bending frequency of the plate vs. number of monomials in the MLS basis function.

5.1.4 The Scaling Parameter c

It is clear from results evinced in Fig. 6 that the dependence of the first four bending frequencies upon c is not monotonic. Whereas $c = 10$ provides very good values of the first two flexural frequencies, $c = 15$ is needed for computing accurately the higher frequencies which involve complicated deformation patterns.

5.1.5 Number of Quadrature Points

We have plotted in Fig. 7 the variation of the first four bending frequencies with the number of quadrature points used to evaluate various integrals in the MLPG formulation. 36 quadrature points suffice for computing

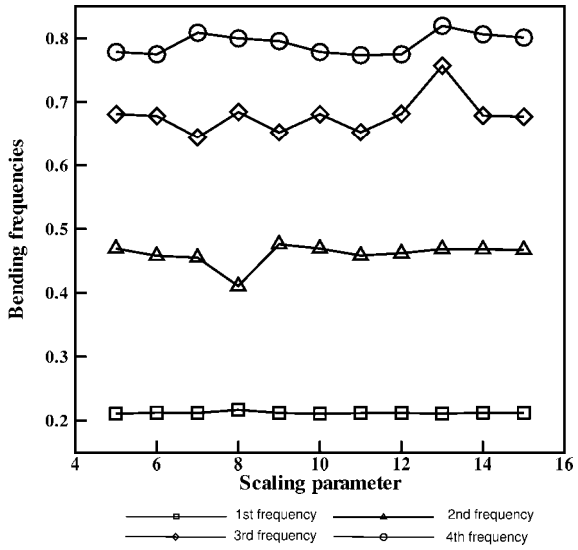

Figure 6 : Bending frequency of the plate vs. the scaling parameter, c.

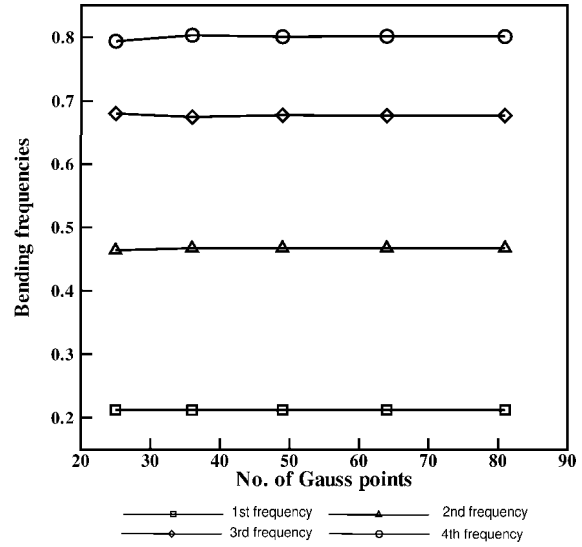

Figure 7 : Bending frequency of the plate vs. number of Gauss points.

the 4th flexural frequency. Our experience with computing results for plates of different aspect ratios and higher frequencies suggests that 64 Gauss points without any partitioning of the domain of integration are sufficient.

5.2 Forced Response of a Plate

The forced response of a clamped square isotropic plate with $h/a = 0.1$ has been analyzed by the Newmark family of methods with $\beta = 0.25$ and $\gamma = 0.5$ and also by the Wilson-θ method with $\theta = 1.37$. Thus both integration techniques are unconditionally stable. Results computed with the MLPG method are compared with those obtained from the 3-dimensional analysis of the problem by using the commercial FE code ANSYS and a uniform mesh of $20 \times 20 \times 3$ 20-node brick elements. We used the consistent mass matrix with the MLPG method and a lumped mass matrix in the FE analysis of the problem. The material and geometric properties used are the same as for the free vibration problem. We have compared the time histories of the centroidal deflection w of the plate and of the axial stress σ_{xx} at the centroid of the top surface of the plate computed by the two methods and for each of the two time-dependent pressure loads $= q_0 g(t)$ applied on the top surface. These quantities are nondimensionalized as

$$\overline{w} = \frac{100Eh^3}{12q_0a^4(1-\nu^2)}w,\ \overline{\sigma}_{xx} = \left(\frac{h}{a}\right)^2 \frac{\sigma_{xx}}{q_0}. \tag{48}$$

5.2.1 Simple Harmonic Load

We first set $g(t) = \sin 5000t$ and $\Delta t = 2.0 \times 10^{-7}$s for the Newmark and the Wilson-θ methods. For $K = 5$, $M = 169$, $m = 15$, $N_Q = 81$ and $c = 15$, the computed centroidal deflection and the axial stress vs. time t are plotted in Figs. 8 and 9 respectively. For most values of t the three curves in both Figs. overlap. One can thus conclude that the MLPG solution agrees very well with the FE solution. The axial stress at the centroid of the top surface was computed with the plate equations.

5.2.2 Transient Load

We now set $g(t) = H(t-0) - H(t - 2 \times 10^{-3}\text{s})$ where H is a Heaviside step function. Thus a uniform pressure q_0 is applied to the top surface of the plate for the first 2 ms. The MLPG method is used to compute the transient response with and without damping but no damping was used in the FE analysis. The damping matrix in the MLPG formulation equaled $0.005 \int_{S_\alpha} v^T \tilde{V} dS$ where v^T is the matrix of test basis functions and $\tilde{V}$ the matrix of trial basis functions. The time step was set equal to 2×10^{-7}s for the MLPG and the FE solutions. Time histories till $t = 5$ ms of the centroidal deflection and the axial stress at the centroid of the top surface of the plate have been plotted in Figs. 10-13; results in Figs. 10 and 11 are without damping, and those in Figs. 12 and 13 are with damping. Again the MLPG solution with the

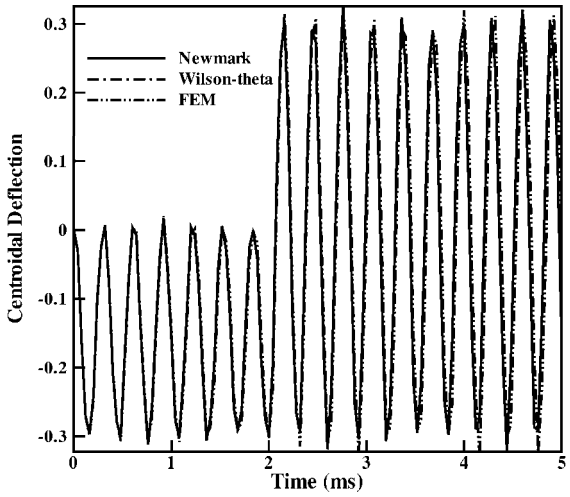

Figure 8 : Centroidal deflection vs. time (The three curves essentially overlap each other)

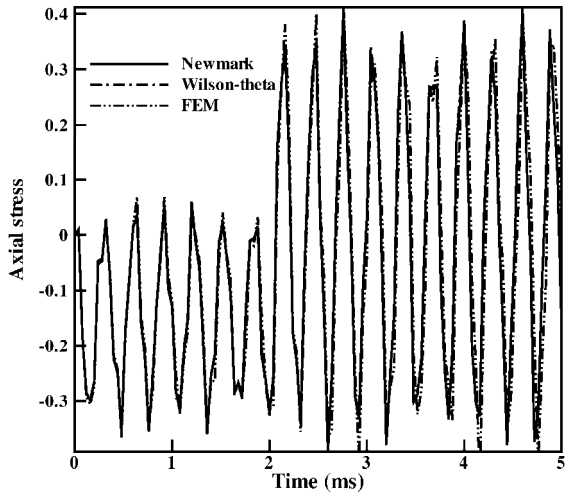

Figure 9 : Axial stress at the centroid of the top surface (The three curves are very close to each other) vs. time

HOSNDPT matches very well with the FE solution of the corresponding 3-dimensional problem.

6 Conclusions

We have used the MLPG method and a higher order shear and normal deformable plate theory to study the natural frequencies and the forced response of a rectangular plate subjected to different edge conditions. No shear correction factor is used, and all domain integrals are evaluated by using the full quadrature rule. Transverse stresses are evaluated from equations of the plate theory.

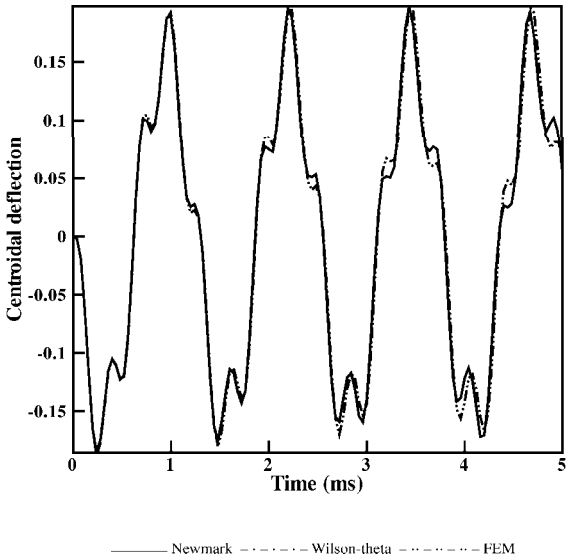

Figure 10 : Centroidal deflection vs. time (The three curves are hardly distinguishable).

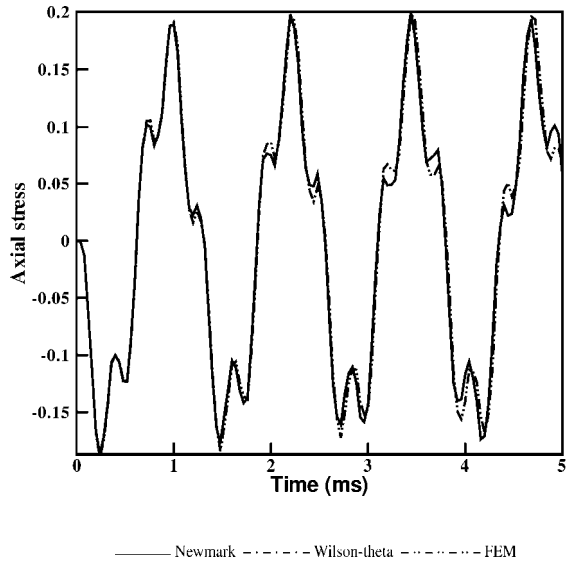

Figure 11 : Axial stress at the centroid of the top surface vs. time (The three curves are very close to each other).

Computed frequencies and the transient response under time-dependent loads are found to agree very well with the corresponding results available in the literature and also computed by the FE analysis of the three-dimensional problem. For the same accuracy of results, the number of degrees of freedom employed with the MLPG method is considerably less than that with the FEM. Whereas the MLPG method requires only the lo-

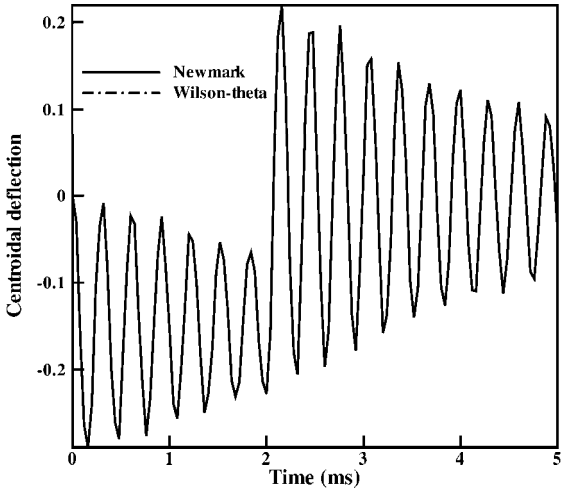

Figure 12 : Centroidal deflection vs. time (The two curves overlap each other)

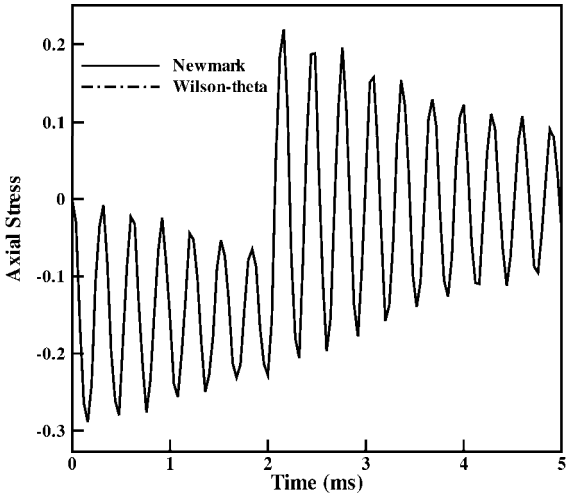

Figure 13 : Axial stress at the centroid of the top surface vs. time (The two solutions coincide with each other).

cations of nodes, the FEM also requires the nodal connectivity which is time consuming even for a regular 3-dimensional rectangular domain considered here. The computation of the mass matrix, the stiffness matrix and the load vector takes more CPU time in the MLPG method than that in the FEM. Furthermore, the mass and the stiffness matrices in the MLPG method are not symmetric but are generally symmetric in the FEM.

Results presented in Tables 1 through 6 evince that frequencies computed by the Galerkin FEM are higher than their corresponding analytical values. However, those computed by the MLPG method do not exhibit this property.

For an incompressible linear elastic material, first ten frequencies for a simply supported square plate computed by the MLPG method and the HOSNDPT are compared below in Table 7 with the analytical solution of Srinivas and Rao (1970) augmented by Batra and Aimmanee (2003). It is clear that the present approach does not exhibit the locking phenomenon prevalent in the FEM.

Acknowledgement: The work was partially supported by the Office of Naval Research grant N00014-98-1-0300 to Virginia Polytechnic Institute and State University with Dr. Y.D.S. Rajapakse as the cognizant program manager. L. F. Qian's work was also supported by the China Scholarship Council.

References

Atluri S.N. and Shen S.P. (2002a): *The Meshless Local Petrov-Galerkin (MLPG) Method*. Tech Science Press.

Atluri S.N. and Shen S.P. (2002b): The Meshless Local Petrov-Galerkin (MLPG) Method: A Simple & Less-costly Alternative to the Finite Element and Boundary Element Methods. *CMES: Computer Modeling in Engineering & Sciences*, Vol. 1, pp. 11-51.

Atluri S.N. and Zhu T. (2000): The Meshless Local Petrov-Galerkin (MLPG) Approach for Solving Problems in Elasto-statics. *Computational Mechanics*, Vol. 25, pp. 169-179.

Atluri S.N., Kim H.G. and Cho J.Y. (1999): A Critical Assessment of the Truly Meshless Local Petrov-Galerkin (MLPG) and Local Boundary Integral Equation (LBIE) Methods. *Computational Mechanics*, Vol. 24, pp. 348-372.

Atluri S.N. and Zhu T. (1998): A New Meshless Local Petrov-Galerkin (MLPG) Approach in Computational Mechanics. *Computational Mechanics*, Vol. 22, pp. 117-127.

Batra, R.C. and Aimmanee S. (2003): Missing Frequencies in Previous Exact Solutions of Free Vibrations of Simply Supported Rectangular Plates, *Journal of Sound and Vibration*, Vol. 265, No. 4, (to appear).

Batra R.C. and Ching H.K (2002): Analysis of Elastodynamic Deformations near a Crack/Notch Tip by the Meshless Local Petrov-Galerkin (MLPG) Method.

Table 7 : First 10 natural frequencies $\overline{\omega} = \omega\sqrt{\rho/G}$ for a SSSS square isotropic plate with h/a = 0.3 and ν = 0.499. G is the shear modulus. An * denotes in-plane mode of vibration

	1	2	3	4	5	6	7	8	9	10
MLPG	0.7760	0.9423*	1.3202*	1.8539*	2.480	2.8130*	3.3523	3.6367	4.0983	4.7632
Analytical	0.7771	0.9425*	1.3329*	1.885*	2.4779	2.827*	3.4126	3.7699	4.072	4.7124

CMES: Computer Modeling in Engineering & Sciences, 3(6), 731-742.

Batra R.C. and Vidoli S. (2002): Higher-order Piezoelectric Plate Theory Derived from a Three-dimensional Variational Principle. *AIAA Journal*, Vol. 40, pp. 91-104.

Batra R.C., Vidoli S. and Vestroni F. (2002): Plane Wave Solutions and Modal Analysis in Higher Order Shear and Normal Deformable Plate Theories. *Journal of Sound and Vibration*, Vol. 257, pp. 63-88.

Belytschko T., Lu Y.Y. and Gu L. (1994): Element-free Galerkin Methods. *Int. J. Num. Meth. Eng.*, Vol. 37, pp. 229-256.

Chati M.K. and Mukherjee S. (2000): The Boundary Node Method for Three-dimensional Problems in Potential Theory. *Int. J. Num. Meth. Eng.*, Vol. 47, pp. 1523-1547.

Ching H.K. and Batra R.C. (2001): Determination of Crack Tip Fields in Linear Elastostatics by the Meshless Local Petrov-Galerkin (MLPG) Method. *CMES: Computer Modeling in Engineering & Sciences*, Vol. 2(2), pp. 273-289.

Freund R.W. (1994): The Look-ahead Lanczos Process for Nonsymmetric Matrices and Its Applications. *Proceedings of the Coynelius Lanczos International Centenary Conference*, SIAM, Philadelphia, PA, pp. 33-47.

Gu Y.T. and Liu G.R. (2001): A Meshless Local Petrov-Galerkin (MLPG) Method for Free and Forced Vibration Analyses for Solids. *Computational Mechanics*, Vol. 27, pp. 188-198.

Iyengar K.T., Chandrashekhara K. and Sebastian V.K. (1974): On the Analysis of Thick Rectangular Plates. *Ingenieur Archiv.*, Vol. 43, pp. 317-339.

Kant T. and Hinton E. (1980): Numerical Analysis of Rectangular Mindlin Plates by Segmentation Method. Civil Engineering Department, Report:C/R365/80, University of Wales, Swansea.

Kant T. (1982): Numerical Analysis of Thick Plates. *Computer Methods in Applied Mechanics and Engineering*, Vol. 31, pp. 1-18.

Kant T. and Swaminathan K. (2001): Free Vibration of Isotropic, Orthotropic and Multiplayer Plates Based on Higher Order Refined Theories. *Journal of Sound and Vibration*, Vol. 241(2), pp. 319-327.

Kim H.G. and Atluri S.N. (2000): Arbitrary Placement of Secondary Nodes, and Error Control, in the Meshless Local Petrov-Galerkin (MLPG) Method. *CMES: Computer Modeling in Engineering & Sciences*, Vol. 3, pp. 11-32.

Kocak S. and Hassis H. (2002): A Higher Order Shear Deformable Finite Element for Homogeneous Plates. *Engineering Structures*, (in press).

Lancaster P. and Salkauskas K. (1981): Surfaces Generated by Moving Least Squares Methods. *Meth. Comput.*, Vol. 37, pp. 141-158.

Lee K.H., Lim G.T. and Wang C.M. (2002): Thick Levy Plate Re-visited. *International Journal of Solids and Structures*, Vol. 39, pp. 127-144.

Liew, K.M., Hung, K.C. and Lim M.K. (1995): Three-dimensional Vibration of Rectangular Plates: Effects of Thickness and Edge Constraints. *Journal of Sound and Vibration*, Vol. 182, pp. 709-727.

Lin H. and Atluri S.N. (2000): Meshless Local Petrov-Galerkin (MLPG) Method for Convection-diffusion Problems. *CMES: Computer Modeling in Engineering & Sciences*, Vol. 1(2), pp. 45-60.

Long S. and Atluri S.N. (2002): A Meshless Local Petrov-Galerkin Method for Solving the Bending Problem of a Thin Plate. *CMES: Computer Modeling in Engineering & Sciences*, Vol. 3(1), pp. 53-64.

Mindlin R.C. and Medick M.A. (1959): Extensional Vibrations of Elastic Plates. *Journal of Applied Mechanics*, Vol. 26, pp. 145-151.

Qian L.F., Batra R.C. and Chen L.M. (2003): Elastostatic Deformations of a Thick Plate by using a Higher-Order Shear and Normal Deformable Plate Theory and Two Meshless Local Petrov-Galerkin (MLPG) Methods. *CMES: Computer Modeling in Engineering & Sciences*, Vo. 4, pp. 701-712.

Senthilnathan N.R., Lim K.H., Lee K.H and Chow S.T. (1987): Buckling of Shear Deformable Plates. *American Institute of Aeronautics and Astronautics Journal*, Vol. 25, pp. 1031-1036.

Srinivas S., Rao A.K. and Rao C.V. (1969): Flexure of Simply Supported Thick Homogeneous and Laminated Rectangular Plates. *ZAMM*, Vol. 49, pp. 449-458.

Srinivas S., Rao C.V. and Rao A.K. (1970): An Exact Analysis for Vibration of Simply Supported Homogeneous and Laminated Thick Rectangular Plates. *Journal of Sound and Vibration*, Vol. 12, pp. 187-199.

Srinivas S., and Rao, A.K. (1970): Bending Vibration and Buckling of Simply Supported Thick Orthotropic Plates and Laminates. *International Journal of Solids and Structures*, Vol. 6, pp. 1463-1481.

Srinivas S. and Rao A.K. (1973): Flexure of Thick Rectangular Plates. *J. Appl. Mech.*, Vol. 39, pp. 298-299.

Vidoli S. and Batra R.C. (2000): Derivation of Plate and Rod Equations for a Piezoelectric Body from a Mixed Three-dimensional Variational Principle. *J. Elasticity*, Vol. 59, pp. 23-50.

Warlock A., Ching H.K., Kapila A.K. and Batra R.C. (2002): Plane Strain Deformations of an Elastic Material Compressed in a Rough Rectangular Cavity. *International Journal of Engineering Science*, Vol. 40, pp. 991-1010.

Whitney J.M. and Pagano N.J. (1970): Shear Deformation in Heterogeneous Anisotropic Plates. *Journal of Applied Mechanics*, Vol. 37, pp. 1031-1036.

Yang J.S. and Batra R.C. (1995): Mixed Variational Principles in Nonlinear Piezoelectricity. *International Journal of Nonlinear Mechanics*. Vol.30, pp. 719-726.

Yuan F.G. and Miller R.E. (1992): Improved Rectangular Element for Shear Deformable Plates. *Journal of Engineering Mechanics, ASCE*, Vol. 118, pp. 312-328.

Appendix

Expressions for the first seven orthonormalized Legendre polynomials defined on $\left[-\frac{h}{2},\ \frac{h}{2}\right]$ are

$$
\begin{aligned}
L_0(z) &= \frac{1}{\sqrt{h}},\\
L_1(z) &= 2\sqrt{\frac{3}{h}}\frac{z}{h},\\
L_2(z) &= \frac{1}{2}\sqrt{\frac{5}{h}}\left[12\left(\frac{z}{h}\right)^2-1\right],\\
L_3(z) &= \sqrt{\frac{7}{h}}\left[-3\left(\frac{z}{h}\right)+20\left(\frac{z}{h}\right)^3\right],\\
L_4(z) &= \frac{3}{\sqrt{h}}\left[\frac{3}{8}-15\left(\frac{z}{h}\right)^2+70\left(\frac{z}{h}\right)^4\right],\\
L_5(z) &= \sqrt{\frac{11}{h}}\left[\frac{15}{4}\left(\frac{z}{h}\right)-70\left(\frac{z}{h}\right)^3+252\left(\frac{z}{h}\right)^5\right],\\
L_6(z) &= \sqrt{\frac{13}{h}}\left[-\frac{5}{16}+\frac{105}{4}\left(\frac{z}{h}\right)^2-315\left(\frac{z}{h}\right)^4+924\left(\frac{z}{h}\right)^6\right],\\
L_7(z) &= \sqrt{\frac{15}{h}}\left[-\frac{35}{8}\left(\frac{z}{h}\right)+\frac{315}{2}\left(\frac{z}{h}\right)^3-1386\left(\frac{z}{h}\right)^5+3432\left(\frac{z}{h}\right)^7\right],\\
&\cdots
\end{aligned}
\tag{A-1}
$$

For $K=7$ the matrix d_{ij} appearing in equation (3) is given by

$$
d_{ij}=\frac{2}{h}\begin{bmatrix}
0 & 0 & 0 & 0 & 0 & 0 & 0 & 0\\
\sqrt{3} & 0 & 0 & 0 & 0 & 0 & 0 & 0\\
0 & \sqrt{15} & 0 & 0 & 0 & 0 & 0 & 0\\
\sqrt{7} & 0 & \sqrt{35} & 0 & 0 & 0 & 0 & 0\\
0 & 3\sqrt{3} & 0 & 3\sqrt{7} & 0 & 0 & 0 & 0\\
\sqrt{11} & 0 & \sqrt{55} & 0 & 3\sqrt{11} & 0 & 0 & 0\\
0 & \sqrt{39} & 0 & \sqrt{91} & 0 & \sqrt{143} & 0 & 0\\
\sqrt{15} & 0 & 5\sqrt{3} & 0 & 3\sqrt{15} & 0 & \sqrt{195} & 0
\end{bmatrix}
\tag{A-2}
$$